MULTIBODY DYNAMICS SIMULATION AND TESTING OF A SMALL ELECTRONICALLY CONTROLLED TRACKED CHASSIS FOR HILLY AND MOUNTAINOUS TERRAIN

/

丘陵山地小型履带式电控底盘多体动力学仿真与试验

Xiaolian LÜ[1)], Jiankang HUANG[1)], Ruijuan SU[1)], Yang ZHANG[2)], Xiaorong LÜ[*2)]
[1)] College of Mechanical & Electrical Engineering, Chuzhou University, Chuzhou, 239000, China;
[2)] College of Machinery & Electronics, Sichuan Agricultural University, Yaan, 625014, China
** Corresponding author, E-mail: lxrxj2008@163.com*

DOI: https://doi.org/10.35633/inmateh-79-84

Keywords: *Track Chassis; Electronic Control; RecurDyn; Dynamical Model; Testing*

ABSTRACT

To meet the maneuverability and terrain-adaptability requirements of agricultural machinery operating in hilly and mountainous areas, an electronically controlled tracked chassis was designed and developed. Based on a theoretical analysis of chassis terrain-crossing capability and stability, a multibody dynamic model was established using RecurDyn to simulate the dynamic response of the chassis under typical operating conditions. The chassis trajectory and variations in dynamic stability were analyzed. A physical prototype was then manufactured and tested under multiple operating conditions on actual road surfaces. The chassis achieved a maximum straight-line travel speed of 4 km/h on level ground, a maximum uphill and downhill travel speed of 2 km/h, a maximum climbing angle of 18°, a maximum trench-crossing width of 500 mm, and a turning radius not exceeding 675 mm. The simulation and experimental results were in close agreement, with a maximum relative error of 11%, demonstrating the predictive accuracy of the multibody dynamic model. The developed chassis exhibited good terrain-crossing capability and operational stability. This study provides a theoretical basis and technical support for the development and application of small agricultural machinery in hilly and mountainous areas.

中文摘要

针对丘陵山地复杂地形对农机装备机动性与适应性的要求，本文设计开发了一款小型履带式电控底盘。基于多体动力学底盘通过性及稳定性理论分析，运用 RecurDyn 仿真软件构建底盘动力学模型，模拟底盘在典型工况下的动态响应特性，并对其运动轨迹及系统稳定性变化规律进行仿真分析。对研制样机进行实际路况条件下多工况性能测试，当平地直行最大速度为 4km/h，上下坡最大速度为 2km/h 时，最大坡度角为 18°，跨越壕沟最大宽度为 500mm，最小转向半径小于 675mm。仿真与试验结果表明，构建的多体动力学模型具有较高的预测精度，底盘在复杂地形下具有良好的通过性与稳定性，相对误差均≤11%。研究为丘陵山地小型农机装备研发提供了可靠的理论依据与技术支撑。

INTRODUCTION

From the perspective of global agricultural development trends, the efficient utilization of agricultural resources in hilly and mountainous areas has become a crucial direction for countries to enhance comprehensive agricultural productivity and expand production boundaries. In regions with limited arable land and diverse topography, the mechanization of agriculture in hilly and mountainous areas is not only vital for local agricultural modernization but also a key component of national agricultural strategies *(HU et al., 2025; Jin et al., 2023; Jiang et al., 2025)*. Due to the complex terrain and insufficient agricultural infrastructure, the promotion and application of agricultural mechanization in hilly and mountainous areas lag far behind those in plain regions. Accelerating the modernization of agriculture have become urgent problems *(Sun et al., 2024; Xiong et al., 2023; Chen, 2025)*. The small tracked electronic control chassis, with its advantages of low ground pressure ratio and strong terrain adaptability, is conducive to the operation of mountainous mechanized equipment *(Ding et al., 2025; Buzunov et al., 2023; Belloni et al., 2024; Liu et al., 2025; Chen et al., 2024; Zemánek and Neruda, 2021)*.

Xiaolian LÜ, Prof.; Jiankang HUANG, B.S. Stud; Ruijuan SU, M.S. Stud; Yang ZHANG, M.S. Stud; Xiaorong LÜ,Prof.

As the core traveling and load-bearing component of agricultural machinery, the dynamic performance of the chassis is a key technical link that restricts the development of agricultural machinery equipment. Scholars have conducted extensive research on chassis, and obtained many achievements *(Archut et al., 2026; Baek et al., 2020; HIDALGO et al., 2015; Grazioso et al., 2023; Yun et al., 2023; Ugenti et al., 2023; HUANG et al., 2025)*. *Mirosław et al. (2025)* developed a model of an articulated UGV (unmanned ground vehicle), and studies on the influence of clearances in the steering and track systems on the directional stability of articulated tracked UGVs. *Dudzińskiand and Chołodowski (2021)* established an internal resistance model for the tracked chassis to optimize energy efficiency. *Pei et al. (2025)* examines the climbing performance of the crawler harvester chassis to solve the problems of running ability and stability of the chassis of the crawler combine harvester during mechanical operation. *Komissarov (2025)* developed a simulation model of a high speed tracked vehicle power train with step track gear boxes to be inserted as a subsystem into a highly computationally efficient model of the tracked vehicle curvilinear motion. Existing research mostly focuses on chassis structure design and conventional performance testing, and the study of chassis dynamic response laws under complex and variable working conditions in hilly and mountainous areas is still not deep enough. Traditional physical testing has high costs and long cycles, making it difficult to comprehensively and accurately obtain chassis dynamic characteristics. Dynamic simulation technology can effectively compensate for the shortcomings of testing. This article takes the self-designed electrically controlled tracked chassis in hilly and mountainous areas as the research object, systematically conducts dynamic theoretical analysis of chassis operating performance. The research provides technical support for promoting the mechanization and intelligence of agricultural equipment in hilly and mountainous areas.

MATERIALS AND METHODS

Overall Structure and Parameters

This article has completed the modular integrated design of an electronically controlled tracked chassis. The chassis consists of a frame, a track traveling mechanism, a steering system, a braking mechanism, an electric drive unit, a control system, and a power supply. The overall configuration is shown in Fig. 1. The basic technical parameters are shown in Table 1. The chassis uses STC89C52 microcontroller as the main control chip to build a remote wireless remote-control system. The system integrates modules such as speed display, Bluetooth communication, encoder, motor drive controller, drive motor, power battery, and data acquisition. The matching principles of various hardware parameters have been clarified, and the core control logic has been formulated. Implementing closed-loop regulation of driving speed and brake pressure threshold through PID algorithm is to achieve precise steering control. The designed chassis has a driving speed of 2-4 km/h, a maximum climbing ability of 20°, and a maximum crossing trenches width of 550 mm. The chassis has remote control and flexible steering characteristics, which can meet the needs of multi working conditions in hilly and mountainous areas.

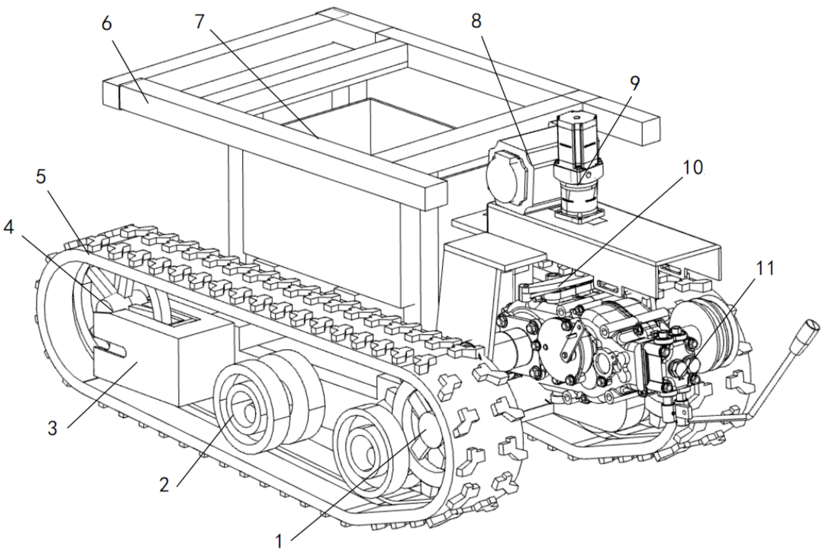

Fig. 1 - The structure diagram of the small tracked electronic control chassis
1 - Drive sprocket; 2 - Support wheel; 3 – Bracket; 4 - Guide wheel; 5 – Track; 6 – Frame; 7 – Controller; 8 - Travel motor; 9 - Steering motor; 10 - Steering mechanism; 11 – Transmission

Table 1

Track Chassis Parameters

Name	Parameter	Name	Parameter
Length × Width ×Height/mm	1000×650×200	Drive sprocket diameter /mm	210
Wheelbase /mm	860	Support wheel diameter /mm	150
Track gauge /mm	470	Guide wheel diameter /mm	190
Track ground-contact length /mm	680	Climbing angle /°	20
Track width /mm	150		

Overall Scheme of the Control System

To achieve wireless remote control and real-time monitoring of the tracked chassis, a measurement and control system was designed with the STC89C52 microcontroller as the main controller. The system primarily consists of a microcontroller minimal system, power module, motor drive module, wireless communication module, and speed monitoring and display module. The overall scheme is shown in Figure 2. The microcontroller minimal system serves as the core control unit, responsible for command reception, logical operations, signal parsing, and motion control. The power module uses a 48 V lithium battery as the primary power source, employing a voltage step-down regulation method to provide 5 V operating voltage for the microcontroller and output stable 24 V through a voltage step-down module, ensuring reliable and stable power supply for the encoder and stepper motor. The motor drive section adopts a dual-channel drive architecture, with the DC brushless motor using the ZM-6750A driver (Operating voltage range: DC32~60 V; Capable of handling peak currents below 50 A); the stepper motor employs the DM-542 driver (Operating voltage range: DC24~50 V; Output current range: 1.0~4.2 A). Wireless communication utilizes the HC-06 Bluetooth module to establish a stable communication link with the mobile app, ensuring reliable transmission of remote control commands and data interaction. Speed monitoring employs the Omron E6B2- CWZ1X rotary encoder, installed at the DC brushless motor shaft end, to collect real-time actual speed data of the driven wheels. The display module uses an LCD1602 screen (Operating voltage range: 4.8~5.2 V), and powered directly by the microcontroller, enabling real-time display of the chassis speed and visualizing the operational status. During system operation, Bluetooth serial assistant of the mobile phone sends control commands, which are transmitted via the Bluetooth module to the microcontroller. After signal parsing and computation, the microcontroller outputs corresponding drive signals to control the motor drivers, thereby enabling functions such as starting, stopping, steering, and speed adjustment of the tracked chassis, ensuring stable system operation, rapid response, and reliable control.

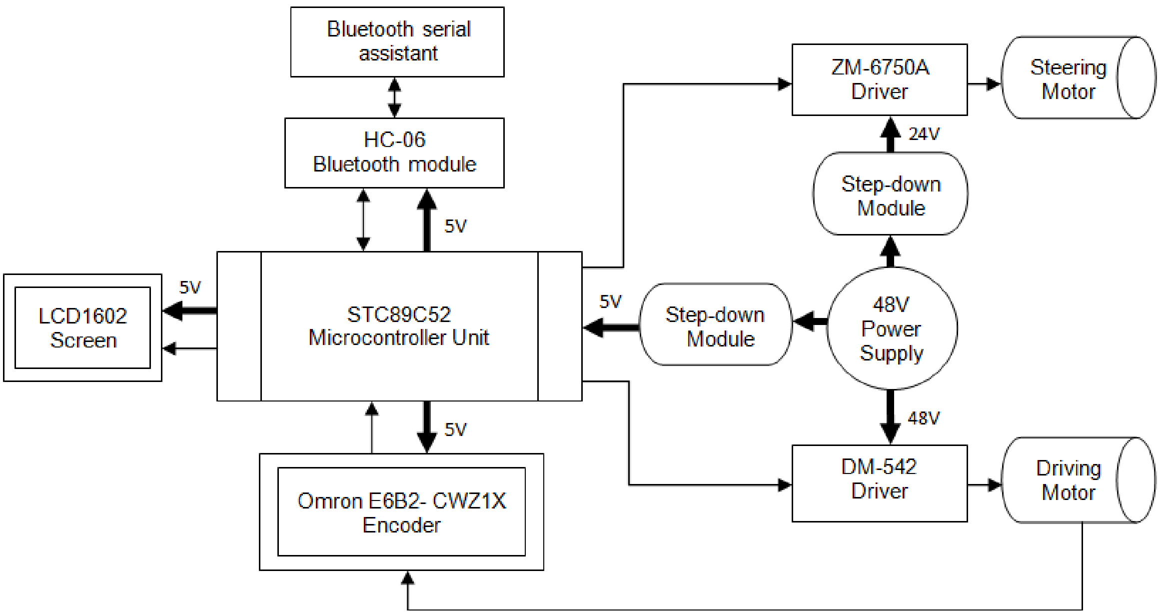

Fig. 2 - The Overall scheme block diagram of control system

Dynamic Performance Analysis of the Chassis

The climbing capability, trench-crossing performance, and steering characteristics of the tracked chassis are key indicators of its operational stability and adaptability to complex terrain. Under idealized operating conditions, mechanical modeling and force analysis of the chassis under different operating conditions provide a theoretical basis for structural design and parameter matching. The forces acting on the chassis during uphill and downhill travel are shown in Fig. 3.

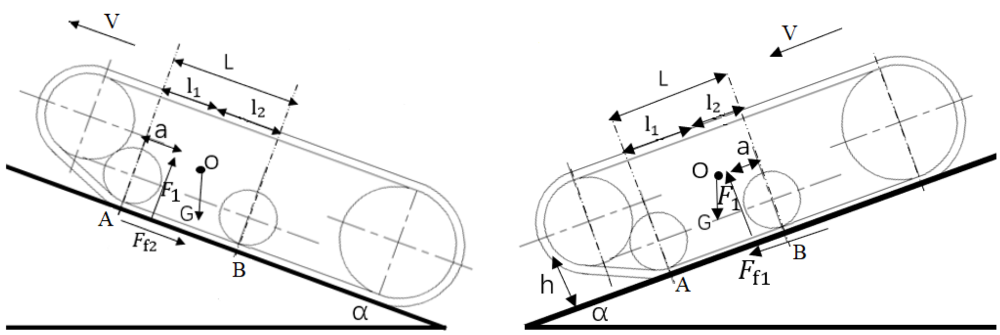

(a) Uphill (b) Downhill

Fig. 3 - Force analysis diagram of the chassis climbing

V-Chassis forward speed, m/s; O-chassis center of mass; G-chassis gravity, N; α - slope, °; h-ground clearance of the center of mass, mm; F_1- ground support force of the chassis, N; a-distance between the support wheel and the support force, mm; L - distance between the support wheel A and the support wheel B, mm; l_1- distance between the support wheel A and the center of mass, mm; l_2- distance between the support wheel B and the center of mass, mm

When the chassis is stable uphill, the force on the vehicle body is balanced, and it can be obtained.

$$\begin{cases} F_1 a - G l_1 \cos\alpha - G h \sin\alpha = 0 \\ F_1 = G\cos\alpha \end{cases} \tag{1}$$

Thus, it can be obtained.

$$a = \frac{l_1 \cos\alpha + \mathrm{h}\sin\alpha}{\cos\alpha} \tag{2}$$

The critical condition for chassis overturning is $a = 0$.

The maximum uphill angle is:

$$\alpha_{max,\mathrm{up}} = \tan^{-1}\frac{l_1}{\mathrm{h}} = 25° \tag{3}$$

The maximum downhill angle is:

$$\alpha_{max,\mathrm{down}} = \tan^{-1}\frac{l_2}{\mathrm{h}} = 22° \tag{4}$$

When the chassis crosses the trench, the force distribution and key geometric parameters are shown in Fig. 4.

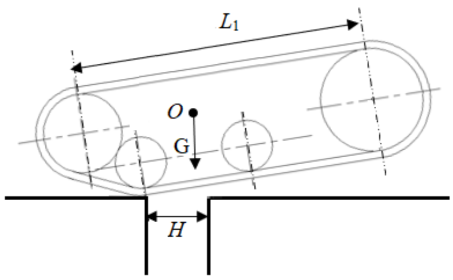

Fig. 4 - Force analysis diagram of tracked chassis crossing trenches

H - maximum width of the chassis crossing the trench, mm; L_1 - distance between the drive sprocket and the guide wheel, mm; O - the center of mass of the chassis; G - chassis gravity, N.

The theoretical maximum trench width of the chassis can be derived:

$$H = \sqrt{(\frac{L_1}{2})^2 + \mathrm{h_1}^2} + r = 581 \text{ mm} \tag{5}$$

where: r - drive sprocket radius, mm; h_1 - guide wheel height, mm.

Mechanical analysis of typical working conditions of chassis steering: the differential steering and unilateral braking steering. The force situation during chassis steering is shown in Fig. 5.

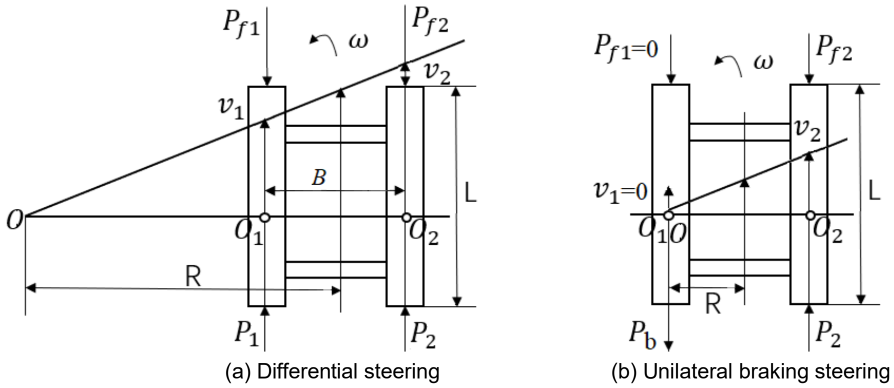

Fig. 5 - Chassis steering performance analysis diagram

O - theoretical steering center of tracked chassis vehicles; O_1,O_2 - instantaneous turning center of the inner and outer track contact sections; v_1,v_2 - the inner and outer track line velocities, m/s; R - steering radius, m; L - the track ground-contact length, m; B - the track gauge, m; P_1,P_2 - the inner and outer track driving force, N; P_{f1},P_{f2} - inner and outer track rolling resistance, N; P_b - track braking force, N; ω - chassis angular velocity, rad/s.

During chassis steering, the following relationship can be obtained:

$$\begin{cases} \omega = \frac{v_2 - v_1}{B} \\ R = \frac{B}{2} \cdot \frac{v_2 + v_1}{v_2 - v_1} \end{cases} \tag{6}$$

where: ω - chassis angular velocity; v_1 - the inner track line velocities; v_2 - the outer track line velocities; B - the track gauge; R - steering radius.

The maximum adhesion of the left and right tracks is:

$$P_{\varphi 1} = P_{\varphi 2} = \frac{1}{2} G\varphi \tag{7}$$

where: $P_{\varphi 1}$ - the maximum adhesion of the left; $P_{\varphi 2}$ - the maximum adhesion of the right; G - the gravity of track chassis; φ - adhesion coefficient.

The rolling resistance of the left and right tracks is:

$$P_{f1} = P_{f2} = \frac{1}{2} G\, f \tag{8}$$

where: P_{f1} - the inner track rolling resistance; P_{f2} - the outer track rolling resistance; G - the gravity of track chassis; f- rolling resistance coefficient.

The steering resistance torque is:

$$M_f = \frac{\mu G L}{4} \tag{9}$$

where: M_f - the steering resistance torque; μ - the average resistance coefficient of steering; G - the gravity of track chassis; L - the track ground-contact length.

The steering torque is:

$$M_1 = \frac{B}{2} P_1 - \frac{B}{2} P_2 \tag{10}$$

where: B - the track gauge; P_1 - the inner track driving force; P_2 - the outer track driving force.

When $M_1 \gg M_f$, the following relationship can be obtained:

$$\frac{L}{B} \ll \frac{2(\varphi - f)}{\mu} \tag{11}$$

In this article, the L of the tracked chassis is designed to be 680 mm and B is 470 mm. The minimum turning radius of the tracked chassis is theoretically less than the sum of the wheelbase and track width. The radius of the chassis unilateral braking steering is 620 mm.

Development of the Multibody Dynamic Simulation Model

To balance dynamic-response fidelity and computational efficiency, the chassis model was simplified to include the main load-bearing frame and the track traveling mechanism. The track traveling mechanism was modeled using the dedicated Track/HM module in RecurDyn, and the constraint relationships among the components were defined, as shown in Fig. 6. The road surface was modeled using the built-in Ground module in RecurDyn. The main simulation parameters are presented in Table 2.

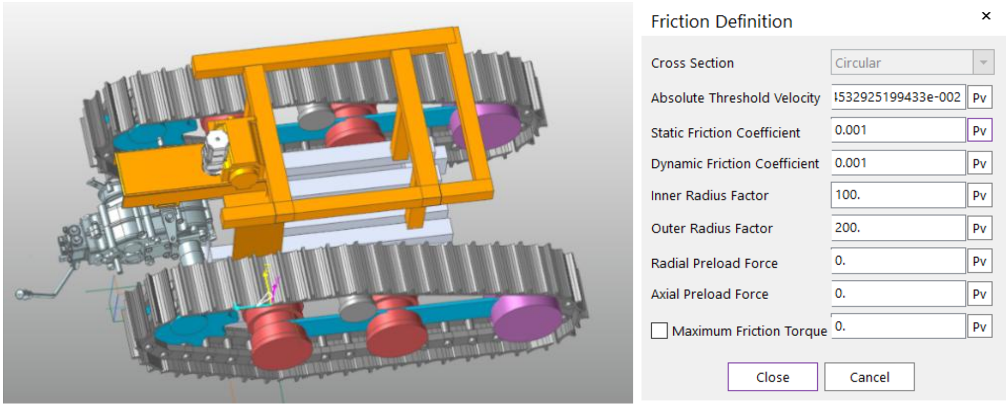

Fig. 6 - Development of the multibody dynamic model of the tracked chassis

Table 2

The road surface characteristic parameters

Parameter	Value
Cohesive deformation modulus of soil k / (N·$m^{-(n+1)}$)	0.417
Frictional deformation modulus of soil $k_{\varphi}/(\mathrm{N}\cdot\mathrm{m}^{-(n+2)})$	2.19×10^{-2}
Soil deformation exponent n	0.5
Soil cohesion c_i/ kPa	4.14×10^{-3}
Internal friction angle / (°)	13
Shear deformation modulus k_s	25
Sinkage ratio	0.05

Chassis performance was comprehensively evaluated in terms of driving stability, terrain-crossing capability, and steering maneuverability using the chassis pitch angle relative to the ground, center-of-mass displacement, center-of-mass velocity, steering angular acceleration, drive-sprocket angular velocity, and chassis angular displacement as evaluation indicators. The simulation conditions were as follows:

(1) Climbing-performance simulation: The slope angle was set to 20°, the travel speed to 2 km/h, and the drive-sprocket angular velocity to ω=5.32 rad/s. The simulation duration was 10 s, with 500 computational steps.

(2) Trench-crossing simulation: The travel speed was set to 3 km/h, and the drive-sprocket angular velocity was set to ω=7.93 rad/s. The STEP function was used to control the variation in drive-sprocket angular velocity STEP (TIME, 1,0,3, -7.93). The simulation duration and number of computational steps were the same as those used in the climbing simulation.

(3) Steering-performance simulation: Two steering modes — single-track braking and pivot steering — were simulated to determine the minimum turning radius. For single-track braking, the right track was braked while the left track continued to travel at 2 km/h, corresponding to a drive-sprocket angular velocity of ω=5.29 rad/s. The function expression for the right drive sprocket was STEP (TIME, 1,0,4,5.29) +STEP (TIME, 5,0,7, -5.29) +STEP (TIME, 8,0,9,5.29), and the speed function for the left drive sprocket was STEP (TIME, 1,0,4,5.29). When performing a Pivot steering, the driving speed was set to 1.5 km/h, the drive sprocket angular velocity ω=3.96 rad/s, the speed function of the right drive sprocket was STEP (TIME, 1,0,2,3.96), and the speed function of the left drive sprocket was STEP (TIME, 1,0,2, -3.96). Pivot steering was achieved by driving the two tracks at equal angular-velocity magnitudes in opposite directions, and the simulation duration and number of computational steps were the same as those used in the preceding simulations.

Field Performance Test Scheme

Test objective: The field tests were conducted to verify the accuracy of the chassis dynamic model, evaluate the dynamic performance of the chassis, and validate the structural design parameters and simulation results. The climbing, trench-crossing, and steering performance of the chassis was investigated.

Test object and method: The test object was the independently developed electronically controlled tracked chassis, and the field-test conditions were consistent with the simulation conditions. Climbing performance was evaluated using the maximum stable climbing angle. The ability of the chassis to travel smoothly on slopes ranging from 5° to 20° was tested. Each operating condition was tested three times and was considered successful only if the chassis completed all three trials. Trench-crossing performance was evaluated using the maximum safe trench-crossing width, with trench widths ranging from 0.30 to 0.55 m.

Each trench width was tested three times and was considered successfully traversed only if all three trials were completed. Steering performance was evaluated using the turning radius during single-track braking. Four steering modes were tested: forward left turn, forward right turn, reverse left turn, and reverse right turn. The largest stable turning radius measured among the four steering modes was taken as the steering-performance value.

RESULTS AND DISCUSSION

Multibody Dynamic Simulation Results

The climbing-performance and trench-crossing simulation results are shown in Figs. 7 and 8, respectively, while the steering-performance results are presented in Fig. 9. Based on the actual steering mode of the chassis, the trajectory of its center of mass during single-track braking on a clay road surface was simulated, as shown in Fig. 10.

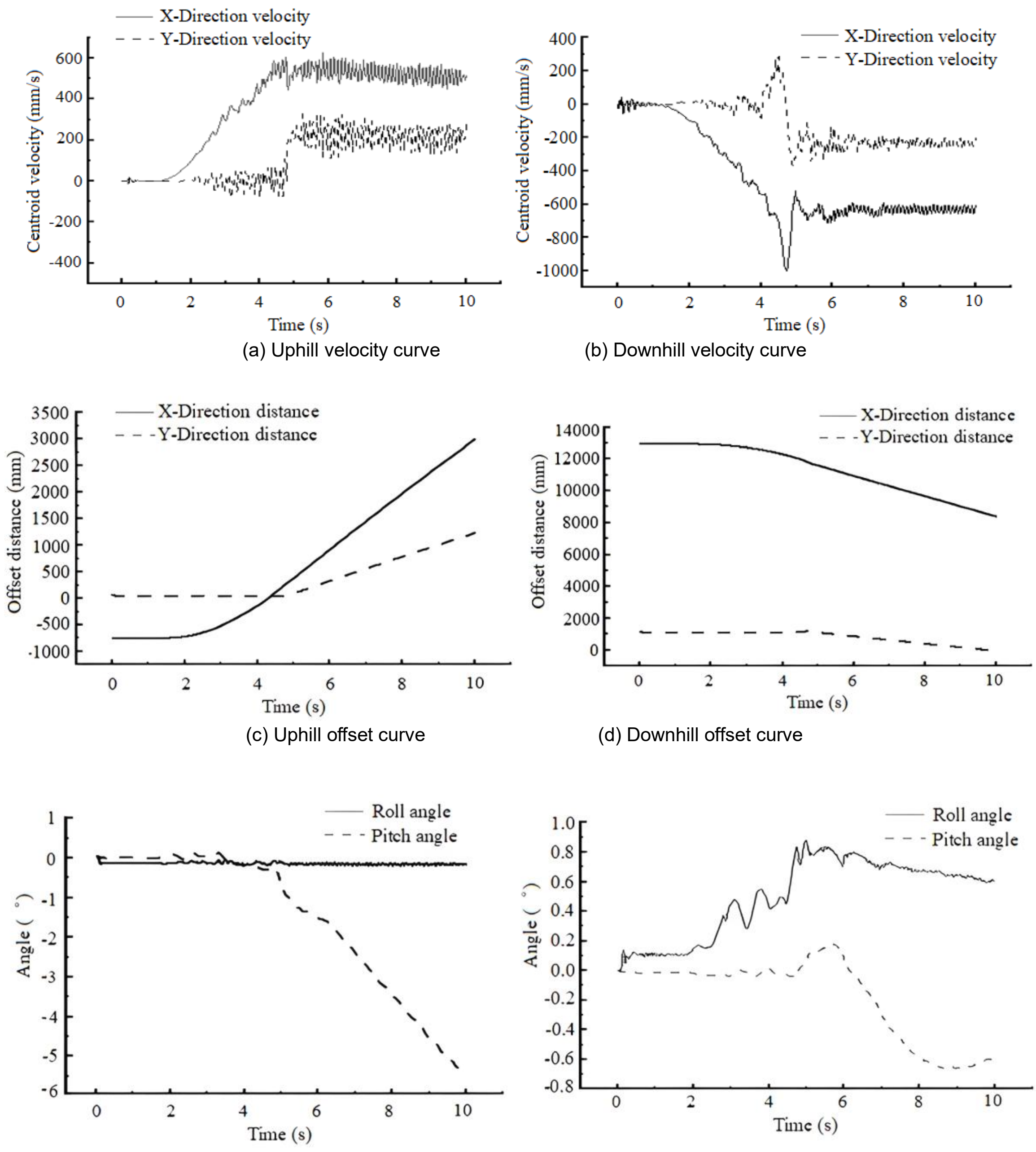

(a) Uphill velocity curve (b) Downhill velocity curve

(c) Uphill offset curve (d) Downhill offset curve

(e) Uphill pitch angle and roll angle (f) Downhill pitch angle and roll angle

Fig. 7 - Dynamic simulation of chassis climbing

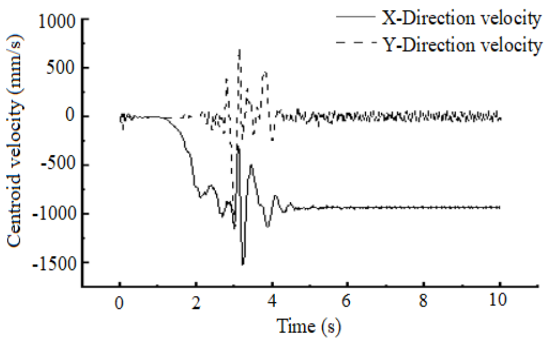

(a) Center of mass velocity curve

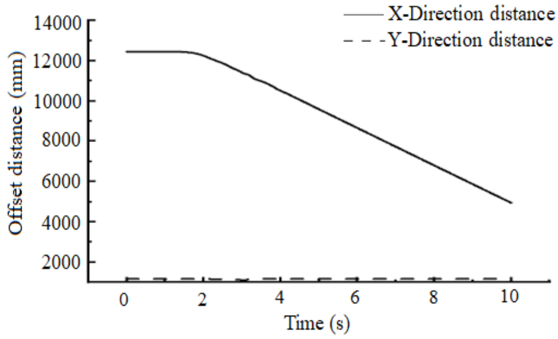

(b) Offset curve

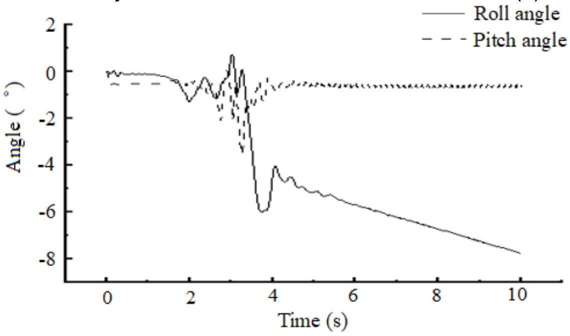

(c) Pitch angle and roll angle

Fig. 8 - Dynamic simulation of chassis trench crossing

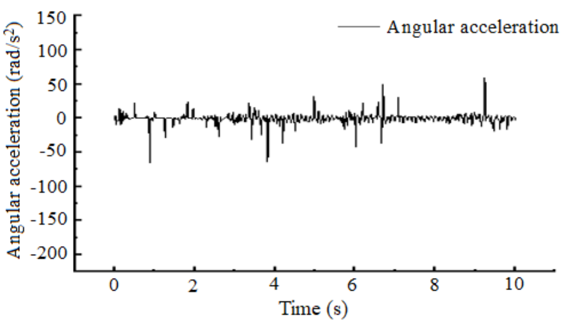

(a) Unilateral braking steering angular acceleration

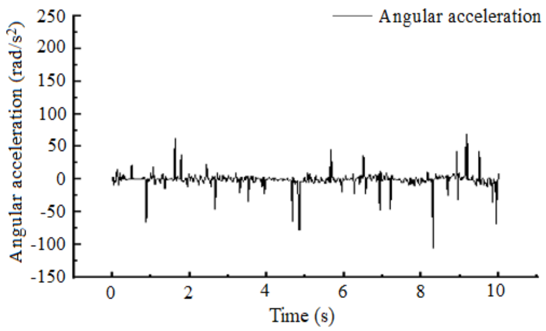

(b) Pivot steering angular acceleration

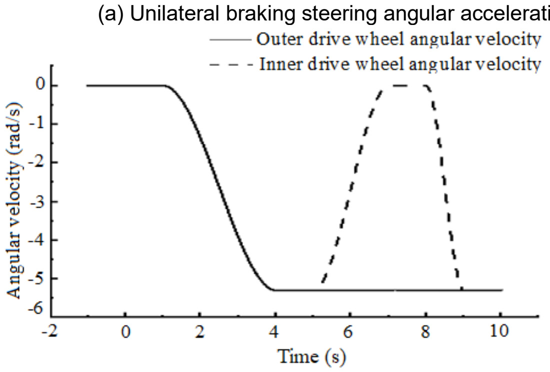

(c) Unilateral braking steering wheel angular velocity

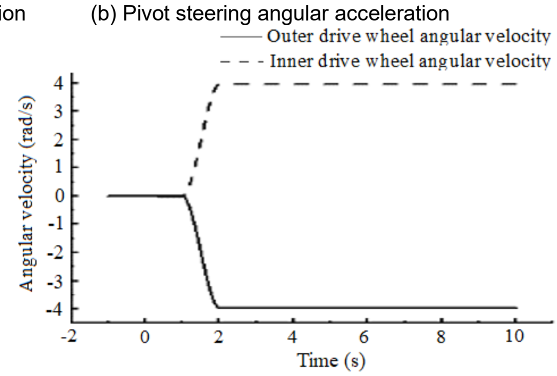

(d) Pivot steering wheel angular velocity

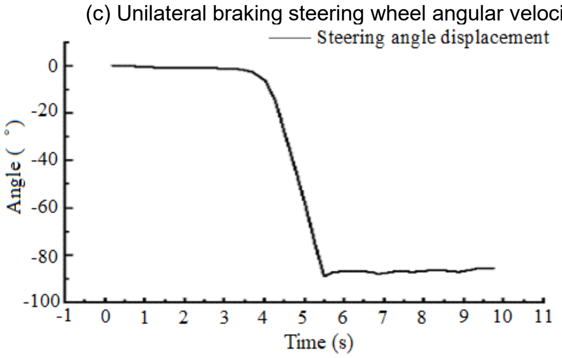

(e) Unilateral brake steering angular displacement

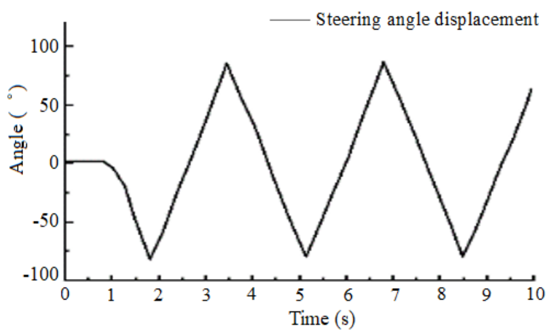

(f) Pivot steering angular displacement

Fig. 9 - Dynamic simulation of chassis steering

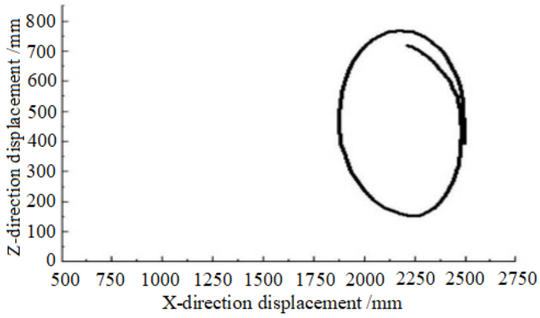

Fig. 10 - Simulated trajectory of the chassis center of mass during steering

The simulation results were analyzed as follows. As shown in Figs. 7(a) and 7(b), during uphill travel, the mean values of Vx and Vy were 0.53 and approximately 0.23 m/s, respectively. During downhill travel, Vx remained relatively stable within the range of 0.5–0.6 m/s, while the mean Vy was 0.23 m/s. The simulated velocity of the chassis center of mass was consistent with the calculated value, supporting the validity of the dynamic model. As shown in Figs. 7(c) and 7(d), at approximately 4 s during both uphill and downhill travel, the displacement in the X-direction began to decrease gradually, while the center of mass exhibited considerable vertical displacement in the Y-direction. After the chassis had fully entered the slope, its center-of-mass displacement continued to increase approximately linearly with time, although the rate of increase decreased slightly. As shown in Figs. 7(e) and 7(f), the pitch and roll angles remained close to zero during most of the uphill process. Near the end of the climb, both angles increased slightly but remained below 6°. During downhill travel, the pitch and roll angles fluctuated more noticeably, with a maximum roll angle of 0.9°. As shown in Fig. 8(a), the center-of-mass velocity fluctuated considerably while the chassis crossed the trench between 2 and 4 s. After trench crossing was completed, the velocity rapidly stabilized, indicating effective drive-speed regulation. As shown in Fig. 8(b), the center-of-mass displacement in the Y-direction remained nearly constant, indicating negligible lateral deviation perpendicular to the direction of travel. The chassis began to enter the trench at 2 s, after which the corresponding vertical-displacement curve decreased approximately linearly. This behavior was consistent with the velocity fluctuations and load variations occurring during trench crossing. As shown in Fig. 8(c), the roll angle exhibited periodic oscillations during trench crossing, while the pitch angle remained below 8° throughout the process. As shown in Figs. 9(a) and 9(b), the angular acceleration varied smoothly during steering, indicating stable steering-power output without marked impact loading. As shown in Figs. 9(c) and 9(d), the single-track braking maneuver proceeded smoothly and steadily. As shown in Figs. 9(e) and 9(f), the chassis initially completed a 90° right turn and subsequently continued traveling in a straight line until the end of the simulation, producing a regular turning trajectory. During pivot steering, the chassis also exhibited a rapid steering response. The simulated trajectory of the chassis center of mass during single-track braking on a clay road surface is shown in Fig. 10. The maximum turning radius was 650 mm, corresponding to an error of 4.85% relative to the theoretical design value.

Field Performance Test Results

The field test results are shown in Figure 11.

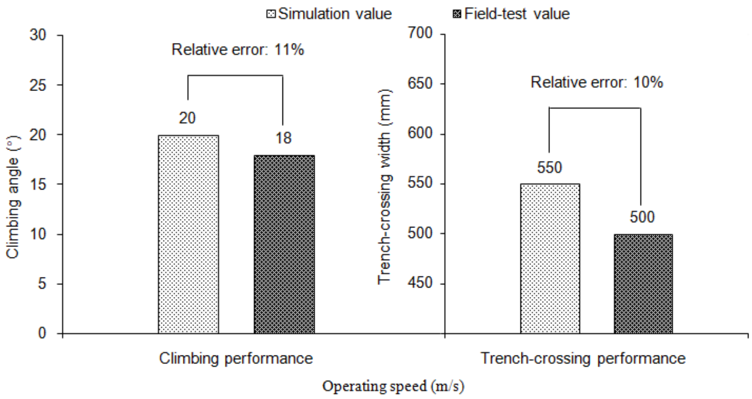

(a) climbing and trench-crossing performance

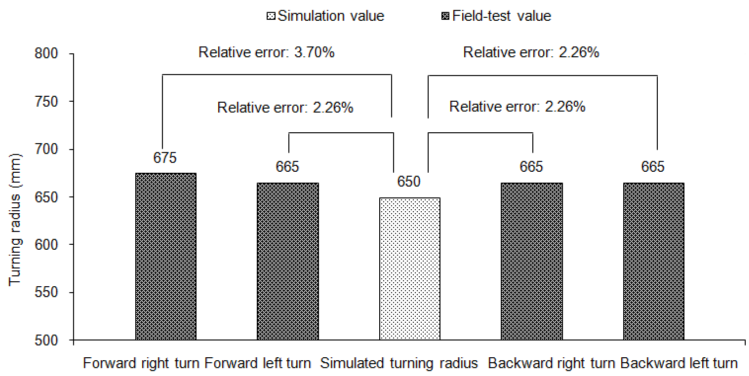

(b) turning radius under different steering conditions

Fig. 11 - Analysis of performance test results for small electronically controlled tracked chassis

Analysis of the experimental results yielded the following findings: (1) The maximum climbing angle of the chassis was 18°, with a relative error of no more than 11% compared with the simulated value. These results validated the accuracy of the climbing dynamic model and demonstrated that the chassis could meet the climbing requirements of operations in hilly and mountainous areas. The deviation was mainly attributed to differences between the actual operating conditions and the idealized model, including track–ground adhesion, track characteristics, and chassis mass distribution. (2) The maximum trench-crossing width measured during the field tests was 500 mm, with a relative error of no more than 10% compared with the simulated value. The results confirmed the reliability of the trench-crossing dynamic model and indicated that the chassis structure could traverse common trench obstacles in hilly and mountainous areas. The deviation was mainly caused by differences in ground conditions, track–ground contact characteristics, chassis attitude, and load distribution between the field tests and the idealized model. (3) The single-track braking tests yielded a maximum turning radius of 675 mm under the different steering conditions, with a relative error of no more than 3.70% compared with the simulated value. The close agreement between the experimental and simulated results validated the developed dynamic model and theoretical analysis method. The steering flexibility and accuracy of the chassis met the requirements for operation in confined spaces in hilly and mountainous areas.

CONCLUSIONS

(1) The multibody dynamic model developed for the electronically controlled tracked chassis under typical operating conditions demonstrated adequate accuracy and applicability. The relative errors for climbing and trench-crossing performance were within 11%, while the relative error in turning radius under different steering conditions was within 3.70%. The model accurately represented the dynamic response of the chassis during operation in hilly and mountainous terrain, providing a reliable theoretical basis for evaluating chassis travel performance and optimizing the track traveling mechanism.

(2) The independently developed electronically controlled tracked chassis met the operational requirements for complex terrain in hilly and mountainous areas. Field-test results showed that the chassis achieved the design targets for climbing, trench crossing, and steering, while maintaining smooth and stable motion. The measured motion parameters under the different operating conditions agreed closely with the theoretical and simulation results. The chassis exhibited good adaptability to uneven terrain and complex ground conditions, thereby confirming the feasibility and practicality of the track traveling mechanism design.

ACKNOWLEDGEMENT

The study was supported by the Natural Science Research Projects of Universities in Anhui Province (2023AH040222), Chengdu Municipal Bureau of Science and Technology Project (2024-YF09-00035-SN), and the SichuanInnovationTeamofChineseNationalModernAgriculturalIndustryTechnologySystem (SCCXTD-2026-21(27)).

REFERENCES

[1] Archut, J. L., & Corves, B. (2026). Non-iterative implicit integration methods with linearization-based equations of motion approximation for real-time multibody vehicle dynamics simulation. *Mechanics Based Design of Structures and Machines, 54(1).* https://doi.org/10.1080/15397734.2026.2623082

[2] Baek, S.H., Shin, G.B., Lee, S.H., Yoo, M., & Chung, C.K. (2020). Evaluation of the slip sinkage and its effect on the compaction resistance of an off-road tracked vehicle. *Applied Sciences*, *10*(9), 317. https://doi.org/10.3390/app10093175

[3] Belloni, M., Vignati, M., & Sabbioni, E. (2024). Analyzing the Effect of Chassis Torsional Flexibility on the Rollover Threshold of a Multi-Purpose Agricultural Vehicle. *Vehicles*, *6*(1), 415-432. https://doi.org/10.3390/vehicles6010018

[4] Buzunov, N.V., Ivanenkov, V.V., Pirozhkov, R.D., Kositsyn, B.B., & Kotiev, G.O. (2023). The method of development of the electronic control system for curvilinear motion of a high-speed tracked vehicle with dual-flow transmission. *Tractors and Agricultural Machinery*, *90*(2), 133-147. https://doi.org/10.17816/0321-4443-312191

[5] Chen, F. (2025). Agricultural mechanization and service innovation in hilly and mountainous areas: An experimental study based on the construction of the Three-in-One demonstration zone in Jiangjin（山地丘陵地区农业机械化与服务创新——基于江津″三化″示范区建设的试验研究）. *Journal of Chinese Agricultural Mechanization*, *46*(9), 72-80. https://doi.org/10.13733/j.jcam.issn.2095-5553.2025.09.010

[6] Chen, Y., Wang, Z., Zhang, H., Liu, X., Li, H., Sun, W., & Li, H. (2024). Investigation of the Traveling Performance of the Tracked Chassis of a Potato Combine Harvester in Hilly and Mountainous Areas. *Agriculture*, *14*(9), 1625. https://doi.org/10.3390/agriculture14091625

[7] Ding, R., Qi, X., Chen, X., Mei, Y., Li, A., Wang, R., & Guo, Z. (2025). Research on the Design of an Omnidirectional Leveling System and Adaptive Sliding Mode Control for Tracked Agricultural Chassis in Hilly and Mountainous Terrain. *Agriculture*, *15*(18), 1920. https://doi.org/10.3390/agriculture15181920

[8] Dudziński, P. A. & Chołodowski, J. (2021). A method for predicting the internal motion resistance of rubber-tracked undercarriages, Pt. 1: a review of the state-of-the-art methods for modeling the internal resistance of tracked vehicles. *Journal of Terrmechanics*, *96*, 81-100. https://doi.org/10.1016/j.jterra.2021.02.006

[9] Grazioso, A., Ugenti, A., Galati, R., Mantriota, G., & Reina, G. (2023). Modeling and validation of a novel tracked robot via multibody dynamics. *Robotica, 41*(10), 3211–3232. https://doi.org/10.1017/S0263574723000966

[10] Hidalgo A, García de Jalón J. (2015). Real-Time Dynamic Simulations of Large Road Vehicles Using Dense, Sparse, and Parallelization Techniques. *Journal of Computational and Nonlinear Dynamics, 10(3): 031005.* https://doi.org/10.1115/1.4028794

[11] Hu, Z., Zhang, M., Luo, W., Pang, Y., Lang, F., & Li, Q. (2025). Advancing agricultural mechanization in China’s hilly and mountainous areas: Key strategies and technological focus（加快中国丘陵山区农机化发展的思考与对策）. *Transactions of the Chinese Society of Agricultural Engineering*,*41*(14), 39-50. https://doi.org/10.11975/j.issn.1002-6819.202412206

[12] Huang, X., Shi, Y., Wang, X., Lin, L., Wang, Y., & Xu, L. (2025). Design and development of a fully electric weeding robot for hilly and mountainous orchards（丘陵山地果园纯电驱动除草机器人研制）. *Transactions of the Chinese Society of Agricultural Engineering*, *41*(18), 28-41. https://doi.org/10.11975/j.issn.1002-6819.202412242

[13] Jiang, Y., Wang, R., Ding, R., Sun, Z., Jiang, Y., & Liu, W. (2025). Research Review of Agricultural Machinery Power Chassis in Hilly and Mountainous Areas. *Agriculture*, *15*(11), 1158. https://doi.org/10.3390/agriculture15111158

[14] Jin, W.C., Wang, O., Yang, M.Y. & Long, T.Y. (2023). The development strategy and path of China’s agricultural mechanization under the goal of building a strong agricultural country（农业强国建设目标下的中国农业机械化发展战略与路径策）. *Issues in Agricultural Economy*, *2023*(10), 13-21. https://doi.org/10.13246/j.cnki.iae.2023.10.007

[15] Komissarov, A.I. (2025). Simulation model of a high speed tracked vehicle powertrain with step track gear boxes. *Tractors and Agricultural Machinery*, *92*(1), 25-34. https://doi.org/10.17816/0321-4443-631516

[16] Liu, Q., Ji, Y.X., Yang, F.Z., Zhang, L.H., Du, Z.X., Liu, Z.J., & Zhu, X.Y. (2025). Development and Validation of Traction Performance for Mountain Tracked Chassis on Slopes（山地履带式底盘坡地牵引性能预测模型构建与试验）. *Transactions of the Chinese Society for Agricultural Machinery*, *56*(5), 597-607. https://doi.org/10.6041/j.issn.1000-1298.2025.05.058

[17] Mirosław, P., Tomasz, M., & Karol, K. (2025). Simulation studies on the influence of clearances on the directional movement stability of articulated tracked unmanned ground vehicles. *Advances in Science*

and Technology Research Journal,*19*(1), 229-24. https://doi.org/10.12913/22998624/194887

[18] Pei, C.N., Dai, F., Shi, R.J., Zhao, W.Y., Zhao, Y.M., Chen, J.Z., Pan, H.F., & Deng, H. (2025). Simulation analysis and test of chassis climbing performance of hilly area crawler quinoa combine harvester(丘陵山地履带式藜麦联合收割机底盘爬坡性能仿真分析与试验). *Agricultural Research in the Arid Areas*, *43*(1), 287-298. https://doi.org/10.7606/j.issn.1000-7601.2025.01.30

[19] Sun, J.B., Zeng, L.K., Ying, J., Zhen, H., Sun, Q., & Meng, X.Z. (2024). Research Status and Prospect of Key Technologies of Agricultural Track Chassis(农业履带底盘关键技术研究现状与展望). *Transactions of the Chinese Society for Agricultural Machinery*, *55*(11), 202-220. https://doi.org/10.6041/j.issn.1000-1298.2024.11.022

[20] Ugenti, A., Galati, R., Mantriota, G., & Reina, G. (2023). Analysis of an all-terrain tracked robot with innovative suspension system, *Mechanism and Machine Theory*, *182*, 105237. https://doi.org/10.1016/j.mechmachtheory.2023.105237

[21] Xiong, Y.S., Si, J.Y., Xie, X.B., Ding, Z., Wang, J.S., & Zhang, L.H. (2023). Development of agricultural crawler traveling device(农用履带行走装置研制). *Journal of Chinese Agricultural Mechanization*, *44*(12), 87-91. https://doi.org/10.13733/j.jcam.issn.2095-5553.2023.12.014

[22] Yun, S., Lee, J., Jang, W., Kim, D., Choi, M., & Chung, J. (2023). Dynamic modeling and analysis of a driving passenger vehicle. *Applied Sciences, 13(10), 5903.* https://doi.org/10.3390/app13105903

[23] Zemánek, T., & Neruda, J. (2021). Impact on the Operation of a Forwarder with the Wheeled, Tracked-Wheel or Tracked Chassis on the Soil Surface. *Forests*, *12*(3), 336. https://doi.org/10.3390/f12030336